

Open-cluster density profiles derived using a kernel estimator

Anton F. Seleznev^{1*}

¹*Astronomical Observatory, Ural Federal University, Mira str. 19, Ekaterinburg 620002, Russia*

Accepted 2015..... Received 2015...; in original form 2015...

ABSTRACT

Surface and spatial radial density profiles in open clusters are derived with the use of a kernel estimator method. Formulae are obtained for contribution of every star into spatial density profile. Evaluation of spatial density profiles is tested against open cluster models from N-body experiments with $N=500$. Surface density profiles are derived for seven open clusters NGC 1502, NGC 1960, NGC 2287, NGC 2516, NGC 2682, NGC 6819 and NGC 6939 by means of 2MASS data and for different limiting magnitudes. The selection of optimal kernel halfwidth is discussed. It is shown that open cluster radius estimates hardly depend on kernel halfwidth. Hints of stellar mass segregation and structural features indicating cluster non-stationarity in the regular force field are found. A comparison with other investigations shows that the data on open cluster sizes are often underestimated. The existence of an extended corona around open cluster NGC 6939 was confirmed. A combined function composed of King density profile for the cluster core and uniform sphere for the cluster corona is shown to be a better approximation of the surface radial density profile. King function alone does not reproduce surface density profiles of sample clusters properly. Number of stars, the cluster masses, and the tidal radii in the Galactic gravitational field for the sample clusters are estimated. It is shown that NGC 6819 and NGC 6939 are extended beyond their tidal surfaces.

Key words: open clusters and associations: general – open clusters and associations: individual: NGC 1502, NGC 1960, NGC 2287, NGC 2516, NGC 2682, NGC 6819, NGC 6939

1 INTRODUCTION

Surface density profiles are traditional tools in investigations of the structure of stellar clusters. Surface density profiles were used for cluster size determination, for example, Sung, Sana & Bessell (2013), Santos-Silva & Gregorio-Hetem (2012), Camargo, Bonatto & Bica (2012). It can be noted that usually surface density profiles were plotted as histograms of star counts, and stochasticity of histograms prevented a reliable cluster size determination. Methods were presented to reduce both stochasticity and asymmetries. Kholopov and Artyukhina performed star counts in the series of overlapping rings of different widths and in overlapping sectors, see, for example, Artyukhina & Kholopov (1962), Kholopov (1963). Djorgovski (1988) proposed an averaging of star counts across several angular bins. Apart from stochasticity, the limited field of view is often the reason for unreliability of cluster size determination.

Cluster density profiles can be compared with different dynamic models in order to reveal the results of different dynamic processes. For example, gravothermal catastrophe in globular clusters becomes apparent by means of post-collapse density profiles (Sosin & King 1995, 1997; Miocchi et al. 2013). Density profiles in the outer cluster parts reveal cluster disruption processes in the outer tidal field, for example, Carraro, Zinn & Moni Bidin

(2007), Küpper et al. (2010), Carballo-Bello et al. (2012). The presence of mass segregation shows an efficiency of stellar encounters; or, in the case of extremely young clusters, preferential birth places of stars with different masses or special features in the cluster formation process: for example, Pang et al. (2013), Goldman et al. (2013), Vesperini, McMillan & Portegies Zwart (2009), Gennaro et al. (2011). Irregularities in the density profiles indicate non-stationarity of a cluster in the regular field (Danilov & Putkov 2012).

The extended sparse outer regions of open star clusters, i.e. cluster coronae, are of special interest. The modern review of arguments in favour of cluster coronae existence was presented in Danilov, Putkov & Seleznev (2014). The cluster coronae can extend over the open cluster tidal surface. Stars leave the cluster through the tidal surface in the vicinity of Lagrange points (see, for example, Küpper, Macleod & Heggie (2008), Küpper et al. (2010)). Part of these stars goes fast at large distances from the cluster and forms the cluster tidal tails. Another part of these stars, before moving to tidal tails, can live in the close cluster vicinity (up to distances of four tidal radii of the cluster in the Galactic gravitational field) for a relatively long time, comparable with the mean lifetime of the cluster (Danilov et al. 2014). It is the cluster corona. The formation of coronae in open clusters and in their numerical models can be explained by the formation of unstable periodic orbits and the large number of retrograde unclosed trajectories in the vicinity of such orbits (Danilov et al. 2014).

* E-mail: anton.seleznev@urfu.ru (AFS)

The detection of the open cluster coroneae is difficult due to low stellar density in the coroneae, and due to fluctuations of the stellar density of the background. The parameters of the open cluster coroneae can be determined more firmly and reliably after identifying probable cluster members, taking into account the data on the stellar proper motions, see, for example, Artyukhina (1970). Danilov, Matkin & Pylskaya (1985) proposed the method of star counts (referred hereafter as DMP), based on the use of the function $N(r)$, the number of stars in the circle of radius r . This method was used by Danilov & Seleznev (1994) for the study of the structure of 103 open star clusters. The method implies the comparison of the cluster field with several fields of the cluster neighbourhood. This requires the study of a very large region around the cluster (with the radius of up to six cluster radii). The use of this method is restricted by large-scale fluctuations of the stellar background density in the cluster vicinity. The goal of the present paper is the use of surface density function $F(r)$, derived with the kernel estimator, for the search of coroneae of the open clusters.

Surface density $F(r)$ is the number of stars per unit area of the celestial sphere (r is the current distance from the cluster centre, R is the radius of the circle (sphere) around the cluster centre).

$$dN = 2\pi r F(r) dr, \quad N = 2\pi \int_0^R F(r) r dr. \quad (1)$$

Spatial density $f(r)$ is the number of stars per unit volume of the coordinate space.

$$dN = 4\pi r^2 f(r) dr, \quad N = 4\pi \int_0^R f(r) r^2 dr. \quad (2)$$

The use of radial density profiles assumes the hypothesis of a spherical symmetry. Both surface and spatial stellar density are connected with the corresponding probability densities.

$$\varphi(r) = \frac{2\pi r}{N} F(r), \quad \int_0^R \varphi(r) dr = 1. \quad (3)$$

$$\psi(r) = \frac{4\pi r^2}{N} f(r), \quad \int_0^R \psi(r) dr = 1. \quad (4)$$

Consequently, methods of probability density evaluation can be used to get surface and spatial density. Such methods were considered by Silverman (1986). The kernel estimator stands out among them by intuitive clarity and relatively simple realization. The essence of the kernel estimator method is the following: every data point in the sample is replaced by some function (kernel) normalized by 1. The result of the probability density is the sum of all kernels divided by the number of sample points N . Estimates of the surface or spatial density are obtained as the sum of kernels, not divided by N . It is very important that the density estimate inherits the properties of the kernel function; for example, continuity and differentiability in the case of kernels used in this paper.

The kernel estimator was used in the previous research for estimates of luminosity function and for deriving and analysing surface density maps in star clusters (Seleznev 1998; Seleznev et al. 2000; Prisinzano et al. 2001; Kirsanova et al. 2008; Seleznev et al. 2010; Carraro & Seleznev 2012).

Merritt & Tremblay (1994) used the kernel estimator and the maximum penalized likelihood estimator for the estimation of density profiles. They showed that the one-dimensional kernel estima-

tor did not suit for a surface density profile construction and a two-dimensional method was needed. Merritt & Tremblay (1994) obtained formulae for a kernel function for the case of the surface radial density profile and got estimates for spatial density solving an Abel equation. They investigated the efficiency of both methods for three important distributions (Plummer, de Vaucouleurs, Michie-King) and showed that the use of an ‘optimal’ kernel halfwidth, determined with the minimization of the integrated mean-square error, led to an unsatisfactory result. Merritt & Tremblay (1994) proposed an empirical selection of kernel halfwidths, namely getting a series of profile estimates and selecting the best version, that is ‘simply looking at plots produced using several different values of the smoothing parameter, and accepting the one that is as smooth as possible without being obviously biased – that is, the smoothest curve that closely follows the mean trend defined by curves computed with much smaller smoothing parameter’. They used both kernel and maximum penalised likelihood methods for deriving surface density profiles for the Coma cluster of galaxies and for the M15 globular cluster.

In the present work, a kernel estimator is used for constructing surface radial density profiles for seven open clusters; and for constructing spatial radial density profiles for the numerical models of the open cluster coroneae obtained by N-body experiments with $N = 500$. The paper is organized as follows. Section 2 is devoted to the development of formulae for surface and spatial density profiles. Spatial density profiles of coroneae of the N-body open cluster models are derived in Section 3. Section 4 contains the description of the surface density radial profiles derivation for seven open clusters and the discussion of the profiles. The estimation of the cluster sizes is discussed in Section 5, the results of the present paper are compared with the data from literature. Section 6 describes an approximation of the cluster radial surface density profiles by King profile, with and without considering the contribution from the cluster corona. The cluster mass and the tidal radii estimates are obtained in Section 7. Conclusions are given in Section 8.

2 KERNEL ESTIMATOR FOR SURFACE AND SPATIAL RADIAL DENSITY PROFILES

To understand the derivation of the formulae better, let us begin with the case of the surface density profile. Consider the plane (x, y) tangent to the celestial sphere at the point of cluster centre O (see Fig. 1). Point S is a projection of a star to the tangent plane, a circle with centre S is the projection of the kernel with halfwidth h ; r_* is the distance of the star from the cluster centre in the projection. The contribution of this star to the surface density profile estimate at the distance r_i from the cluster centre is evaluated. The kernel K_2 (see Eq.(4.5), Silverman (1986)) is used for the calculation of the surface density. This kernel corresponds to the contribution to the surface density as:

$$\Delta F = \begin{cases} \frac{3}{\pi h^2} \left(1 - \frac{\rho^2}{h^2}\right)^2 & \text{with } \rho < h, \\ 0 & \text{with } \rho \geq h. \end{cases} \quad (5)$$

This kernel function (often named as ‘quartic’ kernel) has an advantage in the computational aspect. Namely, this function has high smoothness properties contrary to Epanechnikov kernel, that allow to use a reasonably coarse grid for contouring without introducing appreciable errors (Silverman 1986), it is important especially when plotting two-dimensional maps of surface density. Another one, Gaussian kernel, is excellent in differentiability, but it re-

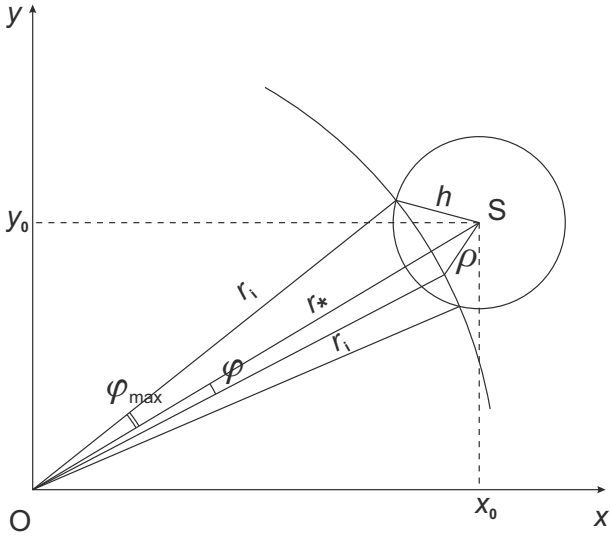


Figure 1. The plane (x, y) is the tangent plane to celestial sphere at the point of the cluster centre O . Point S is a projection of a star to the tangent plane, a circle with centre S is the projection of the kernel with halfwidth h ; r_* is the distance of the star from the cluster centre in the projection. The case $|r_* - r_i| < h$.

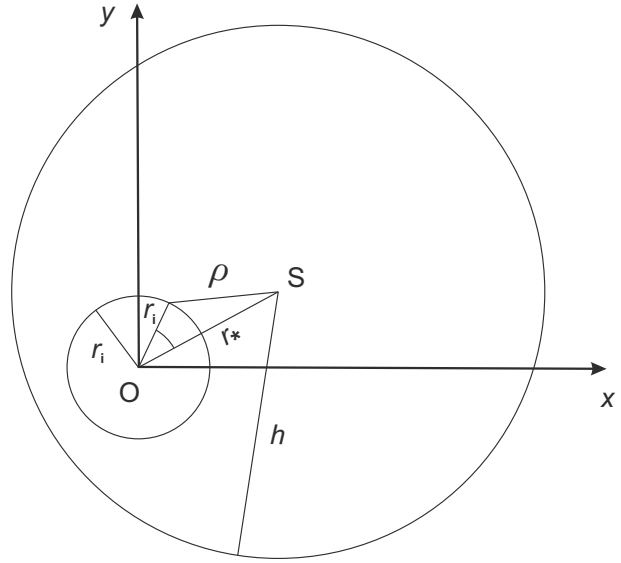


Figure 2. The same as in the Fig.1, but for the case $r_i < h - r_*$.

quires much greater amount of computations (Merritt & Tremblay 1994).

In order to get the contribution of star S into the surface density profile at the distance r_i from the cluster centre, we need to integrate this function by φ over the arc of the circle with radius r_i from $-\varphi_{\max}$ to φ_{\max} (it is the case when $|r_* - r_i| < h$) (see Fig.1). The result is:

$$\begin{aligned} \Delta F(r_i) = & \frac{3}{\pi^2 h^2} \left(1 - \frac{r_i^2 + r_*^2}{h^2}\right)^2 \varphi_{\max} + \frac{6r_i^2 r_*^2}{\pi^2 h^6} \varphi_{\max} \\ & + \frac{12r_i r_*}{\pi^2 h^4} \left(1 - \frac{r_i^2 + r_*^2}{h^2}\right) \sin \varphi_{\max} + \frac{3r_i^2 r_*^2}{\pi^2 h^6} \sin 2\varphi_{\max}, \end{aligned} \quad (6)$$

where

$$\varphi_{\max} = \cos^{-1} \left(\frac{r_i^2 + r_*^2 - h^2}{2r_i r_*} \right).$$

Another situation is possible: when the circle of radius r_i lies inside the circle of the kernel (see Fig.2, $r_i < h - r_*$). In this case we need to integrate Eq.(5) by φ from 0 to 2π . The result is:

$$\Delta F(r_i) = \frac{3}{\pi h^2} \left(1 - \frac{r_i^2 + r_*^2}{h^2}\right)^2 + \frac{6r_i^2 r_*^2}{\pi h^6}. \quad (7)$$

It is easy to show that Eq.(6) and Eq.(7) coincide with Eq.(28b) from Merritt & Tremblay (1994).

The same approach is used for the determination of the contribution of the star into spatial density when the spatial coordinates (x, y, z) of the star are known. The multivariate Epanechnikov kernel (see Eq.(4.4), Silverman (1986)) for three dimensions is used for the case of spatial density. It corresponds to the contribution to spatial density as:

$$\Delta f = \begin{cases} \frac{15}{8\pi h^3} \left(1 - \frac{\rho^2}{h^2}\right) & \text{with } \rho < h, \\ 0 & \text{with } \rho \geq h. \end{cases} \quad (8)$$

The Epanechnikov kernel in the case of three dimensions was selected also due to the computational consideration. It gives more simple equations for the density profile in contrast to the quartic kernel, and requires less number of computations in contrast to the Gaussian kernel. In addition, the difference between the Epanechnikov, quartic, and Gaussian kernels is very little in many aspects (Silverman 1986; Merritt & Tremblay 1994).

Fig.3 shows star S at distance r_* from cluster centre O and three-dimensional kernel with the halfwidth h . The contribution of this star to the spatial density profile at distance r_i from the cluster centre is calculated. Fig.4 shows the sphere with radius r_i around the cluster centre. The coordinate system in Fig.4 was transformed into (ξ, η, ζ) with axis ζ in the direction from the cluster centre to star S . In order to get the required contribution, it is necessary to integrate function Eq.(8) over the segment of this sphere by θ from 0 to 2π and by φ from 0 to φ_{\max} in the case shown in Fig.4 ($|r_* - r_i| < h$) or from 0 to π in the case when the sphere of radius r_i lies inside the sphere of kernel ($r_i < h - r_*$). The result is the following. For the case $|r_* - r_i| < h$:

$$\begin{aligned} \Delta f(r_i) = & \frac{15}{16\pi h^3} \left(1 - \frac{r_i^2 + r_*^2}{h^2}\right) (1 - \cos \varphi_{\max}) \\ & + \frac{15r_i r_*}{32\pi h^5} (1 - \cos 2\varphi_{\max}), \end{aligned} \quad (9)$$

where φ_{\max} is defined just as in Eq.(6). And for the case $r_i < h - r_*$:

$$\Delta f(r_i) = \frac{15}{8\pi h^3} \left(1 - \frac{r_i^2 + r_*^2}{h^2}\right). \quad (10)$$

The algorithm of estimating both spatial and surface density is simple. One must go over the sample of stars, determine at what numbers i (distances r_i) every star contributes to the density and sum up these contributions in accordance with the formulae listed above into array cells with numbers i . Both fixed and adaptive kernel estimator algorithms were examined in the present paper (Silverman 1986; Merritt & Tremblay 1994). An idea of the adaptive kernel algorithm consists in the use of the kernels with different halfwidths depending on the density value. The adaptive kernel estimator gives better estimates in the wings of distribu-

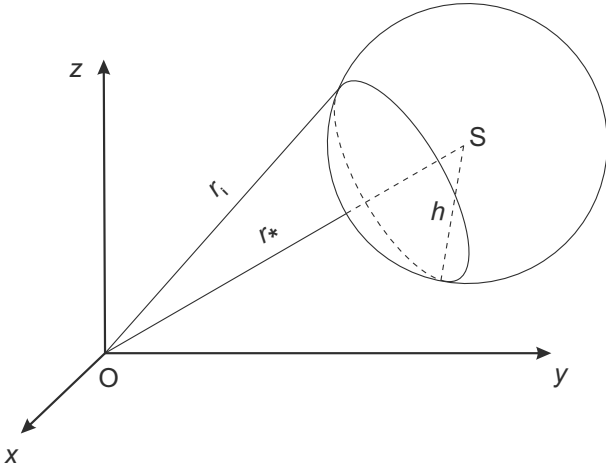


Figure 3. Star S at distance r_* from cluster centre O and three-dimensional kernel with halfwidth h . The case of $|r_* - r_i| < h$.

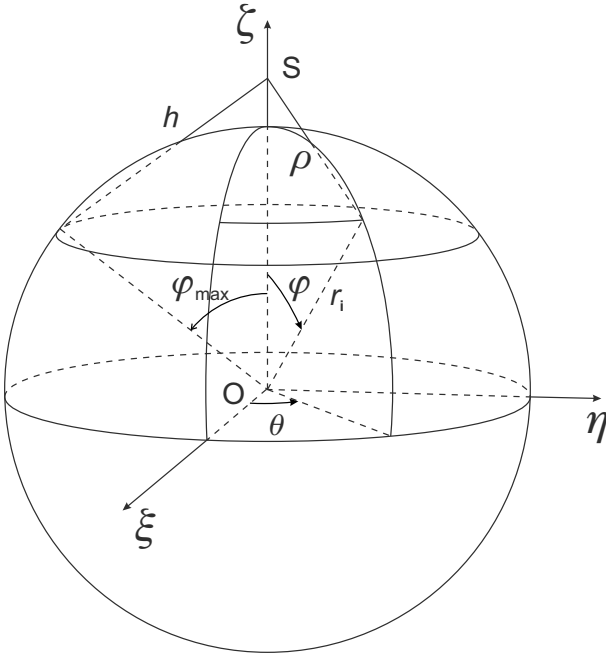


Figure 4. The sphere with radius r_i around cluster centre O. The case $|r_* - r_i| < h$.

tion (Silverman 1986). This algorithm takes two steps: at the first step the pilot density estimate is obtained with the fixed kernel algorithm; this pilot estimate is used at the second step for determination of the kernel halfwidth through factors λ . The adaptive kernel algorithm is described in details in Silverman (1986), and Merritt & Tremblay (1994). In the present paper the same kernel function is used at both steps.

3 SPATIAL DENSITY PROFILES OF CORONAE OF N-BODY OPEN CLUSTER MODELS

At present, the information about the spatial coordinates of stars in star clusters is not available. In order to derive a spatial radial density profile, one must use methods like Zeipel's or Plummer's; or solve the Abel equation numerically. All these methods require

making assumptions about the symmetry type. But the situation will change when GAIA data are available. These data will allow the study of cluster spatial structures directly, at least for the nearest star clusters. Indeed, parallaxes from GAIA data will have standard errors ($5 - 14$) μas for stars in the magnitude range of $V \in (6, 12)$ mag and ($9 - 26$) μas for stars with $V = 15$ mag (Walton et al. 2012). In the case of Pleiades cluster with the distance of 120.2 pc (van Leeuwen 2009) it gives a distance error in the limits of 0.2 pc for bright stars, and of 0.4 pc for stars with $V = 15$ mag. With the linear radius of Pleiades of about 10 pc (van Leeuwen 1980), this accuracy is sufficient for the study of the spatial structure of this cluster. Pleiades have about a hundred of stars in the magnitude range of $V \in (6, 12)$ mag (Belikov et al. 1998).

In the present paper the use of a kernel estimator for the construction of spatial density profiles is illustrated, with spatial coordinates of stars obtained by N-body simulations.

The kernel estimator was used previously for deriving surface radial density profiles of open cluster corona models obtained by numerical N-body experiments, with $N=500$ (Danilov & Dorogavtseva 2008). It was found that the stars, leaving the cluster and forming the cluster corona, shape the surface density distribution close to equilibrium at the distances from the cluster centre in the range from one to three cluster tidal radii (Danilov et al. 2014).

Spatial radial density profiles were derived in the present work with the use of Eq.(9) and Eq.(10) for the same N-body model outputs. The adaptive kernel algorithm was used, because the outer part of the cluster model corona has a very low density. Selection of the optimal kernel halfwidth was made following the recommendations of Merritt & Tremblay (1994). Fig.5 shows the spatial density profiles of the open cluster corona model 1 from Danilov & Dorogavtseva (2008) at the time point of about 150 Myrs (about three violent relaxation times of the model), obtained with the different kernel halfwidths (0.5, 1, 2, 3, 4, and 5 pc from top to bottom). The halfwidth mentioned everywhere in this section is the one used in the pilot estimate for the adaptive kernel method. The stochasticity of the plots in the central region of the cluster is caused by small values of factors λ , that control the kernel halfwidth in the adaptive kernel algorithm ($\lambda < 1$ for $r < 10$ pc). Due to this reason, factors λ were restricted in the present work by 1 from the lower side in the case of spatial density determination.

Fig.6 shows the comparison of fixed and adaptive kernel estimates with the kernel halfwidth $h = 1$ pc (in the case of adaptive kernel estimator $h = 1$ pc refers to the pilot estimate). The adaptive kernel estimate was made with the restricted factors λ . The solid line in this picture shows the adaptive kernel estimate of the spatial density in the corona of model 1 from Danilov & Dorogavtseva (2008) at the time point of about 150 Myrs in the units of pc^{-3} . The tidal radius of this model in the Galactic gravitational field is of about 10 parsecs (see the formula for the tidal radius below in Section 7). The dashed lines show the confidence interval of 2σ width obtained by the smoothed bootstrap method (see Merritt & Tremblay (1994)). This method is based on the Monte-Carlo simulation of multiple secondary samples. Secondary samples are created, which are equal to the original one in size, and which are distributed in accordance with the same density distribution as the original sample. Then the density estimate for the every secondary sample is obtained, using the same kernel estimator. 20 secondary samples were used in this work: it gave density dispersion values for every r_i point. The fixed kernel estimate is shown by open circles. It is clear, that adaptive kernel estimate with $h = 1$

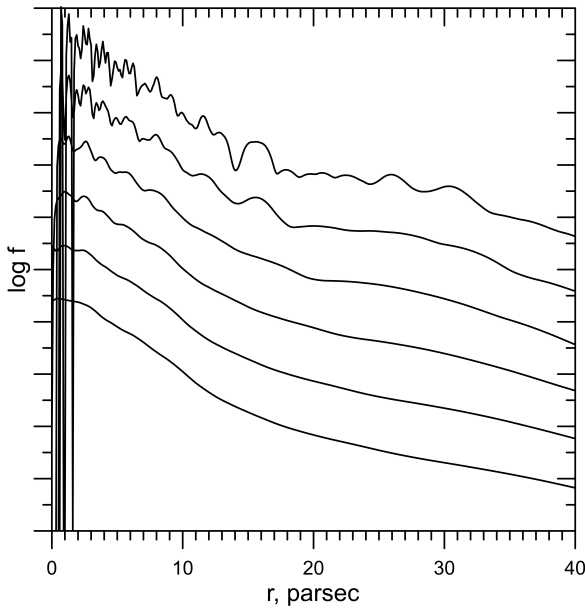


Figure 5. Spatial radial density profiles for corona of model 1 from Danilov & Dorogavtseva (2008), the time point of about 150 Myrs. The kernel halfwidths are 0.5, 1, 2, 3, 4, and 5 pc from top to bottom. The vertical axis shows the logarithm of the spatial density (the density units are pc^{-3}). The major ticks at the vertical axis differ by 1 dex, plots are shifted from each other by the value of 1 dex. The horizontal axis shows the distance from the cluster centre in parsecs.

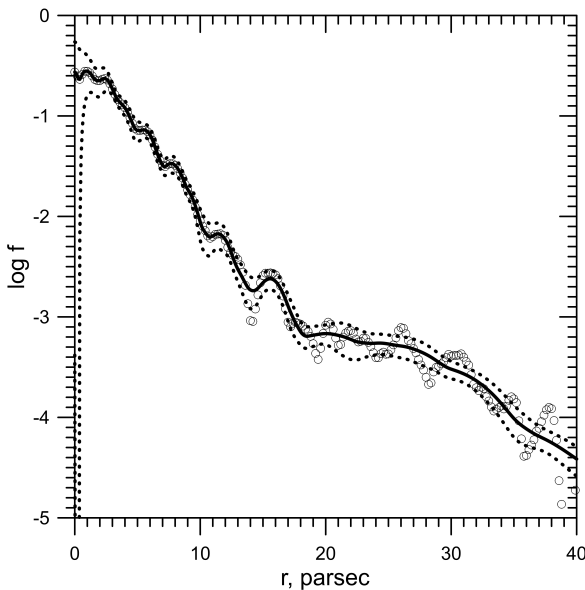


Figure 6. Comparison of the adaptive and fixed kernel estimates of spatial density of the open cluster corona model. The solid line is the adaptive estimate, the dotted lines show the confidence interval of 2σ width, open circles show the fixed kernel estimate. The kernel halfwidth is 1 pc. In the case of adaptive kernel estimator it is the kernel halfwidth for the pilot estimate. The time point is about 150 Myrs.

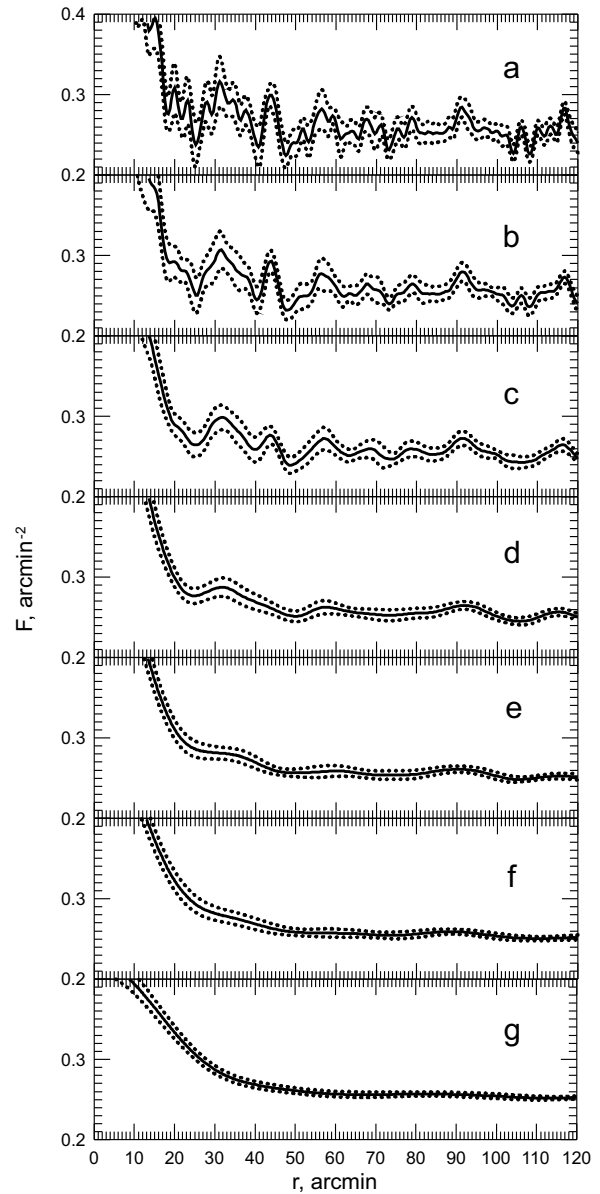


Figure 7. Surface density profiles of open cluster NGC 2287, obtained with different kernel halfwidth values for $J_{\text{lim}} = 13$ mag. (a) $h = 2$ arcmin, (b) $h = 3$ arcmin, (c) $h = 5$ arcmin, (d) $h = 10$ arcmin, (e) $h = 15$ arcmin, (f) $h = 20$ arcmin, (g) $h = 30$ arcmin. The ordinate is the surface density in the units of arcmin^{-2} , the abscissa is the distance from the cluster centre in arcmin. The thick solid line shows the surface density kernel estimate and the dotted lines show the confidence interval of 2σ width, obtained by a smoothed bootstrap method.

pc follows the mean trend defined by the fixed kernel estimate with $h = 1$ pc, and is relatively smooth. The adaptive kernel estimate with $h = 2$ pc has the same characteristics, but is smoother in the central region. Adaptive estimates with $h = 3, 4,$ and 5 pc are biased in the outer part of the corona model. Then the kernel halfwidths of 1 and 2 pc were selected for estimation of spatial density of the open cluster corona model.

The evolution of the spatial density profile with time for the corona of cluster model 1 (Danilov & Dorogavtseva 2008) is shown in the sequences of frames ‘spatial density 1.flv’ (the kernel

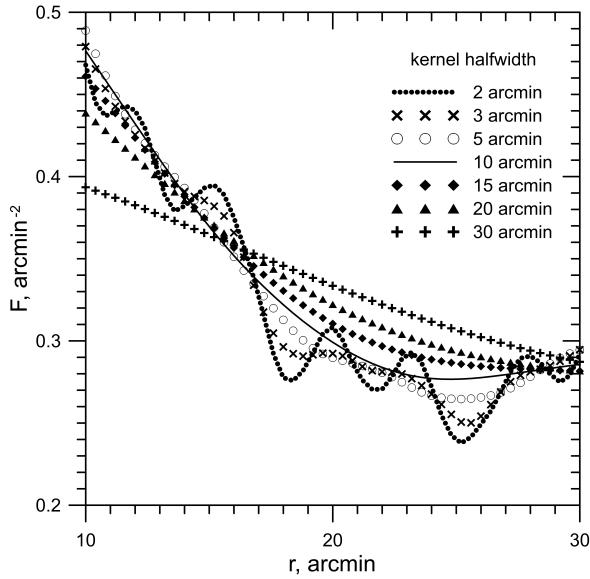


Figure 8. Surface density profiles of open cluster NGC 2287, obtained with different kernel halfwidth values for $J_{\text{lim}} = 13$ mag in the transition region between the cluster core and the cluster halo. The different symbols correspond to the different values of the kernel halfwidth.

halfwidth of 1 pc) and ‘spatial density 2.flv’ (the kernel halfwidth of 2 pc), which are accessible in the online publication of this paper. Each frame is arranged as in Fig.6, but without comparison with the fixed kernel estimate. Each sequence contains 60 frames, the time interval is about 0.05 of the violent relaxation time of this model (Danilov & Dorogavtseva 2008); that is, about 2.5 Myrs. The last frame in the ‘spatial density 1.flv’ is the same as Fig.6. It can be observed that an imaginary upper envelope line for the density profile is stretched to about three tidal radii of the model. This confirms the results of Danilov et al. (2014) on the formation of the quasi-equilibrium density distribution in the cluster corona models. It means that the density profile approaches with time to the upper envelope line which is just the quasi-equilibrium density distribution. This temporal equilibrium in the corona indicates a balance between the numbers of stars entering the corona from inner regions of the cluster and escaping to the corona periphery or beyond it (Danilov et al. 2014).

4 SURFACE DENSITY PROFILES FOR OPEN CLUSTERS

Surface density profiles for seven open clusters were obtained in this work for different limiting magnitudes, J_{lim} , with the data of 2MASS (Scrutskie et al 2006). The sample clusters are listed in Table 1. This table shows galactic coordinates of clusters, their colour excesses, distance modules, distances and ages from Loktin, Gerasimenko & Malysheva (2001), with the last correction of the data (Loktin 2012, private communication). With the exception of NGC 1960 all sample clusters were selected at large galactic latitudes in order to have a more uniform and relatively low stellar background density. Two clusters are young, two clusters are intermediate-aged and three clusters are old. The cluster centre coordinates were taken from the WEBDA database; their accuracy was found sufficient with the large kernel halfwidth used in this work (usually 5 or 10 arcmin).

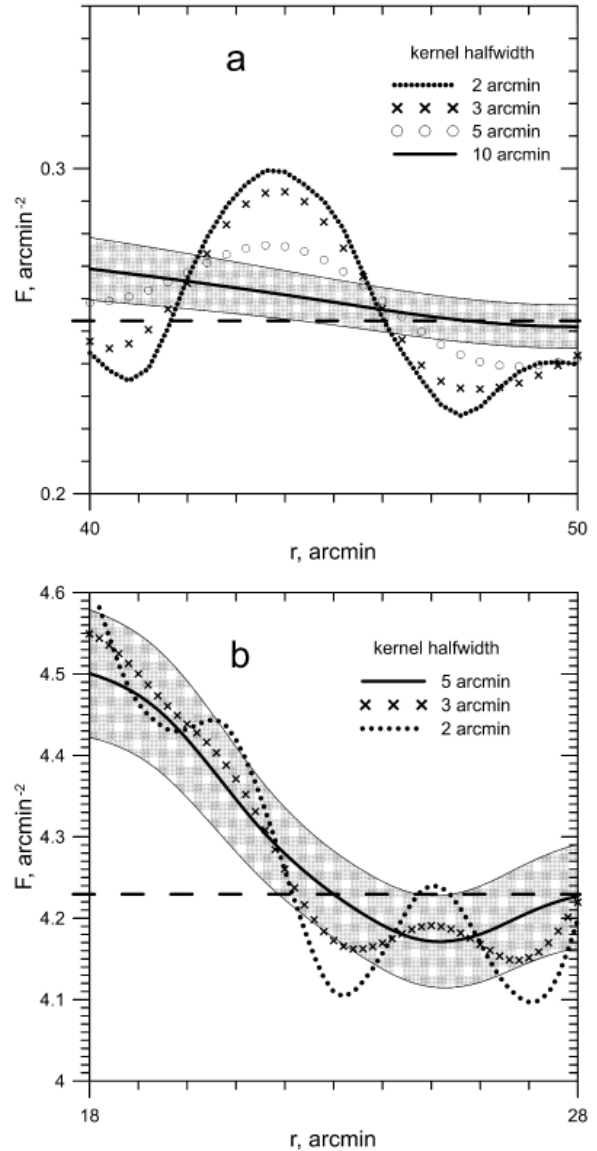


Figure 9. Surface density profiles of the clusters in the region around the cluster boundary, obtained with the different kernel halfwidth values. (a) NGC 2287, $J_{\text{lim}} = 13$ mag; (b) NGC 6819, $J_{\text{lim}} = 16$ mag. Different symbols correspond to different values of the kernel halfwidth. The horizontal dashed line shows the visual estimate of background density (see explanation below in Section 5). Grey bands show the 2σ confidence intervals for profiles with (a) $h = 10$ and (b) $h = 5$ arcmin.

The case of the real open clusters is very different from the case of the open cluster N-body models. The real clusters are observed at the rich stellar background, and the range of the estimates of the surface density values in this case is much smaller, than the range of the estimates of the spatial (or surface) density in the case of model. Due to this reason factors λ , that adjust kernel halfwidth in the adaptive kernel algorithm, have small range also in the case of the real clusters. Factors λ differ from the unity noticeably only in the region of the cluster core. As a result, the adaptive and the fixed kernel estimates of the surface density differ only in the region of the cluster core and coincide completely in the region of the cluster halo and corona. The present work is aimed generally at the study of the outer regions of the open clusters, due to this reason

Table 1. The sample clusters

Cluster name	l , deg	b , deg	E(B-V), mag	Dist. mod., mag	Distance, pc	Log age	h , arcmin	R_f , arcmin
NGC 1502	143.6	7.6	0.76 ± 0.01	9.60 ± 0.14	830 ± 50	7.04 ± 0.05	10	110
NGC 1960 (M 36)	174.5	1.0	0.23 ± 0.04	10.59 ± 0.10	1310 ± 60	7.42 ± 0.20	5	60
NGC 2287 (M 41)	231.1	-10.2	0.03 ± 0.01	9.21 ± 0.10	700 ± 30	8.39 ± 0.07	10	120
NGC 2516	273.9	-15.9	0.10 ± 0.01	8.10 ± 0.11	420 ± 20	8.10 ± 0.04	10	110
NGC 2682 (M 67)	215.6	31.7	0.06 ± 0.01	9.79 ± 0.05	910 ± 20	9.41 ± 0.02	5	115
NGC 6819	74.0	8.5	0.24 ± 0.04	11.87 ± 0.20	2360 ± 200	9.17 ± 0.07	5	55
NGC 6939	95.9	12.3	0.33 ± 0.03	10.45 ± 0.36	1230 ± 200	9.35 ± 0.05	10	160

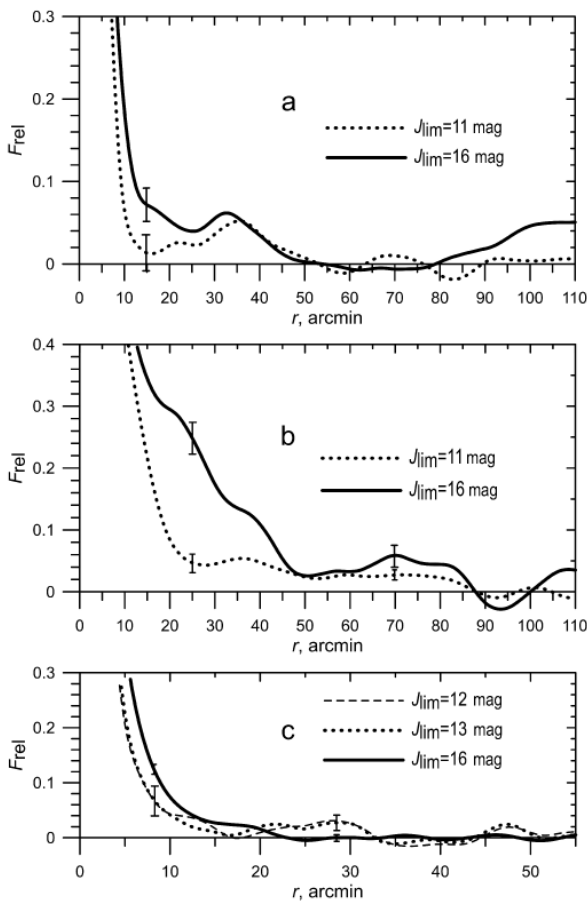


Figure 10. Comparing relative surface density profiles for different limiting magnitudes. a – NGC 1502, b – NGC 2516, c – NGC 6819. Vertical bars show the width of the 2σ confidence interval.

the fixed kernel algorithm is used in the present work for estimation of the surface density of the open clusters.

Let's examine how the result of surface density estimation depends on the kernel halfwidth h . Fig.7 shows the radial surface density profiles for cluster NGC 2287 for $J_{lim} = 13$ mag, obtained with the different kernel halfwidths. It is seen that with the kernel halfwidth decrease the variation of profile increases. Plots 7a, 7b, and 7c vary too greatly. But it is difficult to estimate the degree of bias, because at the region of background ($r > 60$ arcmin) all kernel halfwidths give the same estimate of background density value. The comparison of the surface density estimates in the

region, where the density gradient is changing considerably (the outer part of the cluster core), is the best way for an estimation of the degree of bias in that case. Fig.8 shows the surface density estimates for NGC 2287 obtained with the different kernel halfwidths in the distance range $r \in [10, 30]$ arcmin. It is seen that the curve with $h = 10$ arcmin is smooth, and follows well the mean trend defined by the curves computed with much smaller smoothing parameter. The curves with the larger kernel halfwidths deviate from this trend appreciably. Then the best value of the kernel halfwidth in this case is 10 arcmin, in accordance with recommendations of Merritt & Tremblay (1994).

The same procedure was applied to all sample clusters for all values of the limiting magnitude. One value of the kernel halfwidth was selected for every cluster, with the aim of comparing the surface density estimates derived with different limiting magnitudes. The last two columns of Table 1 show respectively the kernel halfwidth h values accepted for the surface density radial profiles construction of the sample clusters, and radii R_f of fields under consideration. (Important note: in order to estimate the surface density by the kernel estimator with the kernel halfwidth h inside the circle of radius R_f , the coordinates of stars inside the circle with radius $R_f + h$ are needed.)

Tables 2–8 contain data on the surface density profiles obtained in this work: each table contains data for one cluster. All tables are accessible in the online publication of this paper. All tables have the same organization; an example of the first rows of Table 2 for NGC 1502 is given below. The first column contains the distance from the cluster centre in arcmin. Columns 2–5 contain data for limiting magnitude $J_{lim} = 11$ mag: column 2 is the kernel estimate of the surface density radial profile with the kernel halfwidth listed in Table 1; column 3 is the lower boundary of the confidence interval, column 4 is the upper boundary of the confidence interval, column 5 is the surface density histogram with the bin width of 4 arcmin. The histograms with the same bin width are tabulated for all clusters (comparison of kernel estimates and histograms could be useful in some cases). Columns 6–9 contain the same data for limiting magnitude $J_{lim} = 12$ mag; columns 10–13 contain the same data for limiting magnitude $J_{lim} = 13$ mag; columns 14–17 contain the same data for limiting magnitude $J_{lim} = 14$ mag; columns 18–21 contain the same data for limiting magnitude $J_{lim} = 15$ mag; and columns 22–25 contain the same data for limiting magnitude $J_{lim} = 16$ mag. All surface density data are in units of arcmin^{-2} .

The surface density radial profiles for different limiting magnitudes are used in the present work for estimation of the cluster masses, and for evaluation of the segregation of the stars with the different masses (mass segregation).

The nominal completeness limit of 2MASS Point Source Catalogue is 15.8 mag (Scrutskie et al 2006), but in the magnitude range $J \in [15.8, 16.0]$ mag this catalogue is 99% complete for virtually all of the sky (Cutri et al. 2003). At the same time the completeness limit is ~ 0.9 mag fainter at high galactic latitude and ~ 0.4 mag brighter in the galactic plane (Cutri et al. 2003). It means that the completeness limit varies depending on the overall stellar density, and the completeness in the last magnitude range ($J_{\text{lim}} = 16$ mag) can be less than unity and different from one cluster to another.

It may be seen from the results of Merritt & Tremblay (1994), that both kernel and maximum likelihood methods overestimate the surface density in the region of the outer boundary when large values of the smoothing parameter (the kernel halfwidth) are used for the restoration of the Plummer and Michie–King distributions. In that case it is probable that the larger kernel halfwidth would lead to larger cluster dimensions.

The real open clusters do not show the noticeable dependence of the cluster radius on the kernel halfwidth, when the kernel halfwidths listed in Table 1 and smaller ones are used. The possible explanation is that open clusters are projected on a rich stellar background as opposed to the Merritt & Tremblay (1994) models, where stellar background is not taken into account. This is illustrated in Fig.9. Fig.9a shows surface density profiles in the region around the cluster boundary for cluster NGC 2287 for $J_{\text{lim}} = 13$ mag, for kernel halfwidth values of 2, 3, 5 and 10 arcmin. Fig.9b shows surface density profiles in the region around the cluster boundary for cluster NGC 6819 for $J_{\text{lim}} = 16$ mag, for kernel halfwidth values of 2, 3, and 5 arcmin. The cluster boundary (the value of the cluster radius) is determined by the intersection of the cluster surface density profile, obtained with the kernel halfwidth listed in Table 1 and marked in Fig.9 by the thick solid lines, with the line of background density (the dashed line, see explanation below in Section 5). It is clearly noted, that intersection points of the other surface density profiles (obtained with the smaller kernel halfwidth values) with the background density line (near 46–47 arcmin in Fig.9a, and near 22–23 arcmin in Fig.9b) are inside the bands of the confidence interval for profiles with the kernel halfwidth values from Table 1 (the larger ones).

Density profiles obtained with different limiting magnitudes were compared in the present work in order to find the signs of mass segregation in the sample clusters. As the surface density values differ greatly for different limiting magnitudes, relative densities were used, determined by the following formula, where $F_{\text{b}}^{\text{vis}}$ is the visual estimate of the surface density of the stellar background (see explanation in Section 5), and $F(0)$ is the surface density in the cluster centre:

$$F_{\text{rel}}(r_i) = \frac{F(r_i) - F_{\text{b}}^{\text{vis}}}{F(0) - F_{\text{b}}^{\text{vis}}}. \quad (11)$$

The comparison of the relative density profiles for clusters NGC 1502, NGC 2516 and NGC 6819 is shown in Fig.10: Fig.10a is for NGC 1502; Fig.10b is for NGC 2516; and Fig.10c is for NGC 6819. Two types of differences can be marked. The first one is presented in all three clusters: the outer part of the cluster core (or ‘intermediate zone’) is relatively more populous in faint stars. The second type is seen in the case of NGC 2516, where the cluster halo is also more populous in faint stars. All sample clusters show differences of one type or the other. In all cases the relative population of faint stars in the outer cluster regions exceeds the relative population of brighter stars, apart from NGC 6819, where the opposite picture can be seen (Fig.10c).

The Kolmogorov-Smirnov test (KS-test) was performed in order to statistically compare the relative density profiles in Fig.10 (Press et al. 1997). For the profiles from Fig.10a KS-test gives the p-value of $3.8 \cdot 10^{-3}$, and for the profiles from Fig.10b – $3.4 \cdot 10^{-10}$. That is, these profiles are statistically different. For the profiles from Fig.10c, KS-test gives the following results. The profiles with $J_{\text{lim}} = 12$ mag and $J_{\text{lim}} = 13$ mag are not statistically different (the corresponding p-value is 0.9999). The profiles with $J_{\text{lim}} = 12$ mag and $J_{\text{lim}} = 16$ mag are statistically different (the corresponding p-value is $4.1 \cdot 10^{-7}$). The profiles with $J_{\text{lim}} = 13$ mag and $J_{\text{lim}} = 16$ mag are also statistically different (the corresponding p-value is $1.3 \cdot 10^{-6}$).

The mass of sample cluster stars for different magnitudes can be estimated. Transition to absolute magnitudes M_J was made with the data on cluster distances and colour excesses $E(B - V)$ from Loktin et al. (2001) catalogue and with the use of the formulae:

$$E(J - H) = 0.37E(B - V), \text{ and} \quad (12)$$

$$A_J = 2.43E(J - H), \quad (13)$$

where $E(J - H)$ is the colour excess in $(J - H)$ colour index, and A_J is the total extinction in J colour. Formula (12) was taken from Bessell & Brett (1988); formula (13) from Laney & Stobie (1993). Then, the masses of stars were estimated by their absolute magnitudes M_J with isochrone tables downloaded from <http://stev.oapd.inaf.it/cmd> (Bressan et al. 2012) with $Z_{\odot} = 0.019$. The isochrone of $\lg t = 7.0$ was used for clusters NGC 1502 and NGC 1960; the isochrone of $\lg t = 8.3$ was used for clusters NGC 2287, NGC 2516; and the isochrone of $\lg t = 9.3$ was used for clusters NGC 2682, NGC 6819, and NGC 6939. One isochrone is used for the young clusters, one isochrone for the intermediate-aged clusters, and one isochrone for the old clusters. The reason is that only mass–luminosity relation is important in the present work, and this relation changes only negligibly for isochrone with close age values. It is important, that this method does not require the matching of the isochrone to the cluster colour-magnitude diagram (CMD).

The data on stellar masses corresponding to stellar magnitudes in the sample clusters are listed in Table 9. J_{up} in this table denotes the magnitude of the upper end of the cluster sequence in the CMD. In order to find this value, the CMDs ($J, (J - H)$) for sample clusters were plotted by the data of 2MASS in the regions of 10 arcmin around the cluster centre. The uncertainties in this table are due to uncertainties in the cluster distance modules, and in the colour excesses for the clusters (see Table 1). Where the uncertainty interval was determined as asymmetric, the larger value was listed.

The differences in the relative density profiles with the different limiting magnitudes are present in all sample clusters. It is seen from Table 9 that, at least in the young and intermediate-age clusters, there is a large mass spectrum: then we can explain the differences in the profiles there as the consequence of a mass segregation process. In the case of NGC 6819 the outer part of the cluster core is more populated with faint stars, but the cluster halo is more populous with the brighter stars. However, the difference in the mass between cluster stars in that case is minimal, and this fact has yet to be interpreted.

The sample clusters show the presence of structural irregularities in their density profiles, such as secondary maxima or ‘footsteps’ (‘footstep’ is the same as ‘plateau’). The only exception is NGC 1960. The examples are shown in Fig.11. The typical ‘footstep’ is seen in NGC 2287 near $r = 30$ arcmin, the typical secondary maximum is seen in NGC 6939 near $r = 60$ arcmin. Such

Table 2. Data on surface density radial profiles for NGC 1502. The first ten columns and the first seven rows of the whole table, which is accessible in the online publication of this paper.

NGC 1502									
r, arcmin	Jlim=11 mag				Jlim=12 mag				
	F	confidence	interval	histogram	F	confidence	interval	histogram	
1	2	3	4	5	6	7	8	9	10
0.000	0.259154	0.223405	0.294902	0.497359	0.504841	0.446151	0.563532	0.875352	...
0.200	0.258997	0.223273	0.294722	0.497359	0.504559	0.445912	0.563207	0.875352	...
0.400	0.258527	0.222873	0.294180	0.497359	0.503711	0.445191	0.562231	0.875352	...
0.600	0.257738	0.222203	0.293274	0.497359	0.502291	0.443980	0.560601	0.875352	...
0.800	0.256633	0.221264	0.292003	0.497359	0.500293	0.442272	0.558314	0.875352	...
1.000	0.255221	0.220064	0.290377	0.497359	0.497730	0.440076	0.555384	0.875352	...
1.200	0.253507	0.218610	0.288405	0.497359	0.494615	0.437403	0.551827	0.875352	...
...									

 Table 9. The stellar masses at the boundaries of magnitude intervals in the sample clusters (M_{\odot}). J_{up} is the magnitude of the upper end of the cluster sequence in the CMD (see explanation in the text).

Cluster name	J_{up}	$J = 11$ mag	$J = 12$ mag	$J = 13$ mag	$J = 14$ mag	$J = 15$ mag	$J = 16$ mag
NGC 1502	17.31±0.29	3.35±0.23	1.91±0.33	1.43±0.03	1.15±0.05	0.74±0.06	0.40±0.05
NGC 1960 (M 36)	11.15±0.38	4.29±0.22	2.72±0.14	1.53±0.02	1.32±0.03	0.97±0.05	0.59±0.05
NGC 2287 (M 41)	4.09±0.00	1.95±0.08	1.37±0.04	1.07±0.03	0.83±0.03	0.65±0.02	0.49±0.02
NGC 2516	3.87±0.00	1.35±0.04	1.06±0.03	0.82±0.03	0.64±0.02	0.49±0.02	0.33±0.02
NGC 2682 (M 67)	1.72±0.00	1.67±0.01	1.43±0.01	1.18±0.02	0.94±0.01	0.74±0.01	0.59±0.01
NGC 6819	1.72±0.00	1.71±0.00	1.71±0.00	1.70±0.02	1.50±0.06	1.24±0.05	1.00±0.05
NGC 6939	1.72±0.00	1.71±0.01	1.65±0.08	1.41±0.10	1.15±0.09	0.92±0.08	0.73±0.06

structures can indicate the cluster non-stationarity in the regular field, or stabilizing ejections of the cluster stars into the galactic field: see Danilov (1982, 2005, 2011). The non-stationary processes cause the corona not being radially symmetric, and this, in turn, leads again to the structural irregularities in the radial density profiles.

5 SIZES OF OPEN CLUSTERS

The sizes of open clusters were estimated in the present work in two ways. The first one was by a visual estimate, and it was not an objective method.

In the first step, the mean background surface density line was inferred by analysing the outer part of the field under consideration for every cluster, and for every limiting magnitude range. An approximately flat area in the outer part of the density profile was searched, and the background density line was drawn taking into account an approximate equality of the square of areas between this line and density profile above and below this line. In the second step the cluster radius was estimated as the abscissa of the point of intersection of the density profile and the background density line. An error of this estimate was evaluated as the distance from the intersection point of the confidence interval line with the background density line to the cluster radius point (in many cases the confidence interval intersects the background density line only at one

side of the cluster radius point). An error of the background density estimate was evaluated as half of the confidence interval width at the cluster radius point.

These background density lines are shown in Fig.9 and Fig.11. The visual estimates of the cluster radius R_c and the surface density of stellar background F_b^{vis} , and their uncertainties for every cluster and every limiting magnitude interval are listed in Table 11. The intervals of the cluster radius estimates for every cluster are listed in the second column of Table 10.

The second way is the approximation of the cluster surface density profile by the King surface density distribution (King 1962), and by the combination of the King distribution and the cluster corona component (see the description and the discussion in Section 6). It is important that the visual estimates of the mean background surface density and the estimates of the background density via approximation with the combined function are very close (see Table 11).

Table 10 shows the comparison of visual estimates of open cluster radii both with the data of other authors and with the results of cluster radii estimation by the DMP method when the function $N(r)$ (number of stars in the circle with radius r) is used, and the cluster field is compared with several fields of neighbouring background fields (see above in Introduction). All data in Table 10 are in arcmin.

The second column of Table 10 contains the visual estimates of cluster radius by the surface density profile obtained as described

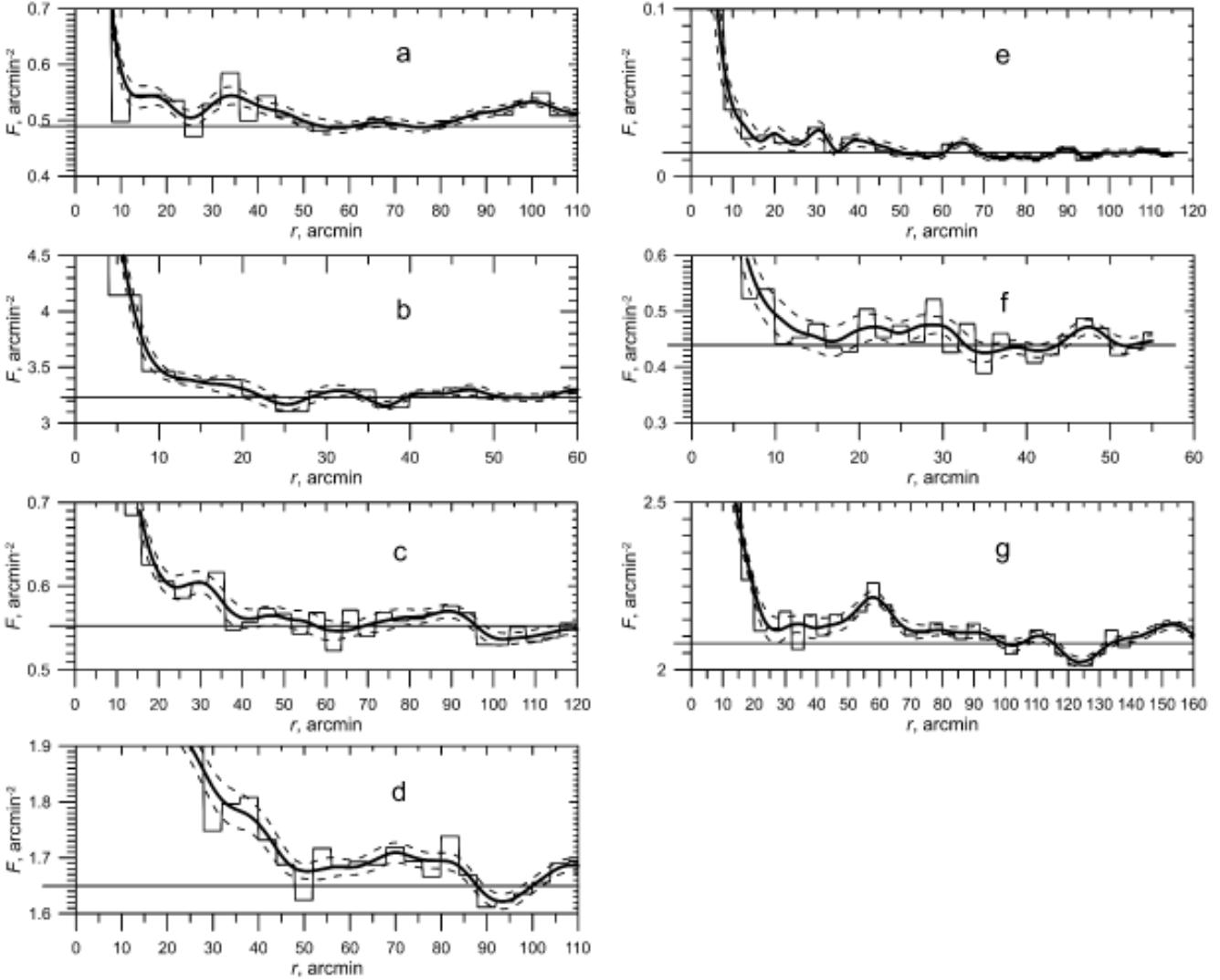


Figure 11. Structural irregularities in the surface density profiles of open clusters. a – NGC 1502 $J_{\text{lim}} = 14$ mag, b – NGC 1960 $J_{\text{lim}} = 16$ mag, c – NGC 2287 $J_{\text{lim}} = 14$ mag, d – NGC 2516 $J_{\text{lim}} = 16$ mag, e – NGC 2682 $J_{\text{lim}} = 11$ mag, f – NGC 6819 $J_{\text{lim}} = 13$ mag, g – NGC 6939 $J_{\text{lim}} = 16$ mag. The solid polygonal lines show the histograms with the bin size of 4 arcmin. The thick solid lines show the surface density estimate, the dashed lines show confidence interval of 2σ width. The solid straight lines show the values of stellar density of background (see explanation in Section 5).

above. The interval shows the scatter of the estimates for the different limiting magnitudes. The number in brackets is the radius of the field used for the density profile construction. The third column shows the cluster radius from the catalogue of Kharchenko et al. (2005). The fourth column shows the data on the sample clusters from the literature, and the fifth column contains the references on the sources of these data. The sixth column contains the cluster radius estimates from Danilov & Seleznev (1994). These estimates were obtained by the DMP method with star counts on photographic plates in B colour band. The number in brackets shows the radius of the cluster field used for the star counts. The seventh column shows the cluster radius estimates obtained by the DMP method with the star counts on the data of 2MASS. The interval shows the scatter of estimates for different limiting magnitudes, and the number in a brackets shows the radius of the cluster field used for the star counts.

The radius estimates by the surface density profile in the case

of NGC 1502, NGC 6819, and NGC 6939 are larger than estimates by star counts with the DMP method. This can be explained by a smaller size of the cluster field used for the DMP star counts. In the case of NGC 1960, NGC 2287, and NGC 2516 the size of the field used for the star counts with the DMP method is larger than the cluster size, and a satisfactory matching by different methods was obtained.

It may be seen from Table 10 that, in the case of NGC 1502, NGC 2287, and NGC 6819, we have in the literature underestimated values of the cluster radius.

Artyukhina & Kholopov (1965) studied the structure of NGC 6939 with the proper-motion-selected cluster members. They found that this cluster has an extensive corona with the radius of about 85 arcmin. In the present work, the surface density profile for NGC 6939 was derived to a distance of 160 arcmin from the cluster centre, and the cluster radius estimate larger than in Artyukhina & Kholopov (1965) was obtained: see Fig.11g. In this

Table 10. Comparison of cluster radii estimates with the data of other authors and with the results of cluster radii estimation by the DMP method (arcmin)

Cluster name	Cluster radius estimate by density profile	Kharchenko et al. (2005) catalog	Data of other authors	Ref.	Danilov & Seleznev (1994) DMP method with plates in B	Radii estimates by DMP method with 2MASS
NGC 1502	52-55 (110)	12.6	5	1	24.8 ± 2.5 (31.08)	37 (45)
NGC 1960 (M 36)	10-23 (60)	16.2	22.9	2	20.1 ± 0.6 (31.08)	
NGC 2287 (M 41)	37-57 (120)	30	30	3		46-50 (60)
NGC 2516	88-92 (110)	42	90	3		87 (95)
NGC 2682 (M 67)	43-57 (115)	18.6	60	4,5		
NGC 6819	16-33 (55)		13	6	24.8 ± 2.6 (31.08)	10-22 (40)
NGC 6939	42-105 (160)		85	7	15.5 ± 1.2 (22.2)	21-26 (30)

(1) Alves et al. (2012), (2) Sanchez & Alfaro (2009), (3) Bergond, Leon & Guibert (2001), (4) Davenport & Sandquist (2010), (5) Balaguer-Núñez et al. (2013), (6) Yang et al. (2013), (7) Artyukhina & Kholopov (1965)

manner the result of Artyukhina & Kholopov (1965) concerning an extensive corona of NGC 6939 can be confirmed. The cluster radius estimate comparable with the result of proper motion cluster membership analysis was obtained in the case of NGC 2682 (Balaguer-Núñez et al. 2013). Kharchenko et al. (2005) used proper motions data for selecting possible cluster members, but these authors obtained smaller cluster radii than in the present work. This is possibly due to the smaller limiting magnitude in their study, and possibly due to using the King (1962) distribution for the cluster structure approximation (see discussion in Section 6).

Nilakshi et al. (2002) performed star counts in the fields of 38 open clusters. They obtained the outer radius of NGC 1960 to be 15.3 arcminutes and the outer radius of NGC 6939 to be 12.7 arcminutes (these values of angular radii were calculated with their data on linear radii and distances). These radii are smaller than the ones obtained in the present paper. In the case of NGC 6939 Nilakshi et al. (2002) couldn't see the cluster boundary near 100 arcminutes, because they were limited by the field with the radius of 30 arcminutes. Their result must be compared rather with Danilov & Seleznev (1994) value, see 6th column of Table 10. In the case of NGC 1960 the reason of underestimation of the radius by Nilakshi et al. (2002) is possibly due to the lower sensitivity of star counts in the rings in comparison with the kernel estimator method. It is worthy to note that the procedure of the outer boundary determination was not described by Nilakshi et al. (2002) in details, and the density profiles (see Fig.1 in Nilakshi et al. (2002)) allow ambiguous radii estimation.

6 APPROXIMATION OF OPEN CLUSTER SURFACE DENSITY PROFILES

The King (1962) function is used very often for approximation of the surface density or the surface brightness profiles of star clusters:

$$F(r) = \begin{cases} k \left[\frac{1}{\sqrt{1 + \left(\frac{r}{r_c}\right)^2}} - \frac{1}{\sqrt{1 + \left(\frac{r_t}{r_c}\right)^2}} \right]^2 & r < r_t, \\ 0 & r \geq r_t. \end{cases} \quad (14)$$

This function was proposed by King for globular clusters but was also widely used for open clusters. In order to take into account stellar background, this formula is supplemented by stellar background density F_b as a constant addition.

Danilov & Putkov (2012) found that the approximation of stellar distribution in open star clusters by the King (1962) function tends to underestimate the number of stars in the cluster compared to the results of star counts. The reason was that the King (1962) function underestimates density values in the region of the cluster corona. Danilov & Putkov (2012) proposed an addition to the King formula. This addition represents the cluster corona as a uniform sphere. The addition into surface density reads:

$$\delta F(r) = 2 \cdot R_2 \cdot \delta f \cdot \sqrt{1 - \left(\frac{r}{R_2}\right)^2}. \quad (15)$$

where R_2 is the radius of the cluster corona, and δf is the spatial density of the cluster corona. This addition should be applied at all radii $r < R_2$.

An approximation of the surface density profiles of the sample clusters was performed in the present work both by the King (1962) function alone (Eq.(14), referred hereafter as 'King model') and by the combined function (a combination of the King distribution for the cluster core Eq.(14) and of the uniform sphere Eq.(15) for the cluster corona, referred hereafter as 'combined model').

The results of the approximation are listed in Table 11, which is accessible in the online publication of this paper. The columns of the table can be divided into three groups. The first group contains visual estimates of the cluster parameters, the second group contains the parameters of the combined model, and the third group contains the parameters of the King model.

The columns of the first group are: (1) the cluster name; (2) the limiting magnitude in J band; (3) visual estimate of the cluster radii R_c in arcmin; (4) its uncertainty; (5) visual estimate of the surface density of the stellar background F_b^{vis} in arcmin^{-2} ; (6) its uncertainty; (7) the estimate of the cluster star number N ; (8) its uncertainty. The estimate of the cluster star number was obtained through the numerical integration of the cluster surface density profile; the uncertainty of this estimate was obtained by integration of the upper and lower confidence interval curves, taking into account the uncertainty in the background density.

The parameters of the combined model were obtained by using the non-linear least-square approximation algorithm by

Marquardt (1963). The parameters of Eq.(14) in the case of the combined model are supplied by the upper index ‘comb’, and in the case of the King model – by the upper index ‘King’. The columns of the second group are: (9) k^{comb} in arcmin^{-2} ; (10) its uncertainty; (11) r_c^{comb} in arcmin ; (12) its uncertainty; (13) r_t^{comb} in arcmin ; (14) its uncertainty; (15) the surface density of background F_b^{comb} in arcmin^{-2} ; (16) its uncertainty; (17) R_2 in arcmin ; (18) its uncertainty; (19) δf in the units of $10^{-3}\text{arcmin}^{-3}$ (this value denotes the number of stars in a cube with the side measured by one arcmin at the cluster distance); (20) its uncertainty. In the combined model, r_t^{comb} can be considered as the cluster core radius, r_c^{comb} has the meaning of the scale parameter for the cluster core, and R_2 is the cluster corona radius. From this perspective, situations when $r_c^{\text{comb}} > r_t^{\text{comb}}$ (see Table 11) are possible. The interpretation of such cases is in the different types of the surface density profiles, namely, in the differences in the transition region between the cluster core and the cluster corona (or the halo). The cluster can have the so-called intermediate zone between the core and the corona (Kholopov 1969; Danilov & Seleznev 1994). The existence of the intermediate zone is normal in rich clusters (Kholopov 1969), and the sample clusters are rather rich. When the intermediate zone exists, the relation of r_c^{comb} and r_t^{comb} is usual. But when the transition between the core and the corona is sharp, the scale parameter for the cluster core is larger than the radius of the core. Such cases occur only in the less populated clusters of the sample, NGC 1502 and NGC 2287.

The following columns of the second group are: (21) the chi-square parameter describing the approximation quality (Marquardt 1963; Press et al. 1997); (22) the cluster star number N_{mod} for the combined model obtained by the analytic expression for the integral of Eq.(1) over the surface density of the combined model $[F(r) + \delta F(r)]$ (see Eq.(14), Eq.(15)); (23) the star number of the cluster corona N_1 ; and (24) the star number of the cluster core N_2 . The number of the cluster corona stars N_1 was obtained by the analytic expression for integral Eq.(1) over the surface density of cluster corona Eq.(15). The number of the cluster core stars was obtained as $N_2 = N_{\text{mod}} - N_1$.

The third group of the columns of Table 11 lists parameters of the King model obtained for the sample clusters by the same algorithm (Marquardt 1963): (25) k^{King} in arcmin^{-2} ; (26) its uncertainty; (27) r_c^{King} in arcmin ; (28) its uncertainty; (29) r_t^{King} in arcmin ; (30) its uncertainty; (31) F_b^{King} in arcmin^{-2} ; (32) its uncertainty; (33) the chi-square parameter; (34) the cluster star number N_{King} for the King model obtained by the analytic expression for integral Eq.(1) over the surface density of the King model, Eq.(14).

The results of the approximation by two models are now compared. The parameter R_2 in the combined model correlates closely with the visual estimate of the cluster radii R_c . In contrast, parameter r_t in the King model does not correlate highly with R_c . It is shown in Fig.12.

Stellar background density F_b^{King} , obtained in the limits of the King model, is usually larger than F_b^{comb} obtained in the limits of the combined model (the latter one is usually very close to the visual estimate of this value). It is clear, when corresponding columns of Table 11 are compared.

One could compare the relative differences of the surface densities of background. The relative difference $(F_b^{\text{vis}} - F_b^{\text{comb}})/F_b^{\text{vis}}$ is generally smaller than 1 percent and not more than 4 percent. The relative difference $(F_b^{\text{comb}} - F_b^{\text{King}})/F_b^{\text{comb}}$ is generally several times larger in the absolute magnitude, and usually negative.

The reason is that the King model does not have an extended corona, and the cluster corona (that is seen clearly in the above Fig.

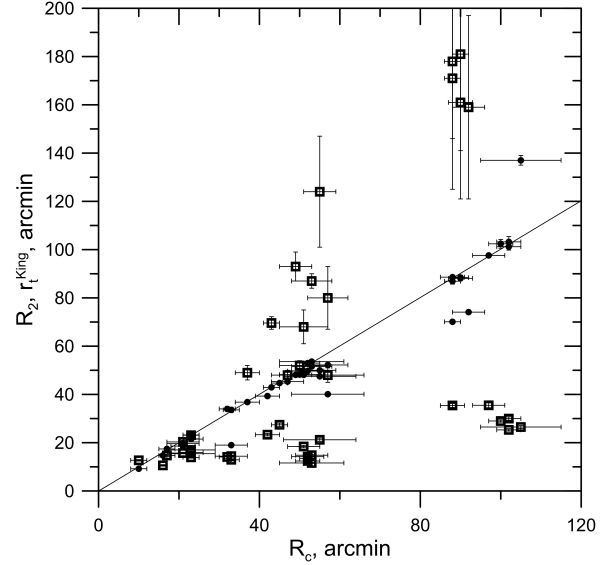


Figure 12. Comparison of the values R_2 and r_t^{King} against the R_c values. The filled circles are R_2 values, and open squares are r_t^{King} values. The straight line shows equal values, for convenience.

10 and Fig.11) is perceived by the approximation algorithm as part of the stellar background. Fig.13 shows the surface density profile for NGC 1502 ($J_{\text{lim}} = 16$ mag), and the fits of this profile both by the King model and by the combined model. It is visible, that the fit by the King model gives the values of the surface density at the distances from the cluster centre between 50 and 80 arcmin (in the background region) larger than the profile values, in contrast to the fit by the combined model. As a result, integration of the density profile of the cluster King model gives a number of stars N_{King} much smaller than N or N_{mod} : usually N_{King} is close to the cluster core star number N_2 in the combined model. In contrast, values of N and N_{mod} are well correlated. This fact is illustrated in Fig.14, where the cluster star numbers in the combined model and in the King model are compared against the cluster star number from the visual estimate of parameters.

Hence, it follows that the King model does not reproduce surface density profiles of the sample clusters very well. This point is supported by the comparison of the chi-square parameters, describing the quality of approximation (Marquardt 1963; Press et al. 1997). Fig.15 shows the chi-square parameters for the King model approximation against the chi-square parameters for the combined model approximation, the latter ones are systematically less. The cluster cores are reproduced by the King function accurately, but the cluster coronae are not. Taking into account that the cluster coronae often have structural irregularities (see Fig.11), it is difficult to reproduce their density profiles by any analytic expression. From this point of view modelling of the cluster corona by a uniform sphere can be reasonable, and gives acceptable results.

7 CLUSTER MASS AND TIDAL RADII ESTIMATES

Having data on the cluster star numbers and on the stellar masses at the boundaries of magnitude intervals, it is possible to estimate the cluster masses. The following algorithm was used. First, the num-

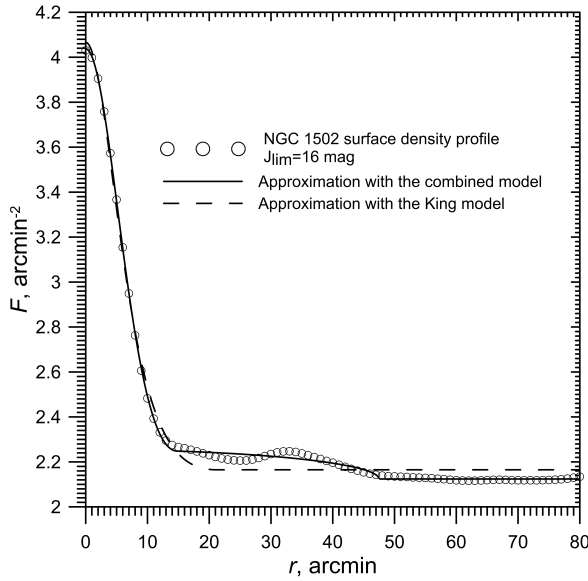


Figure 13. Approximation of surface density profile of NGC 1502 with $J_{\text{lim}} = 16$ by the combined function and the King function.

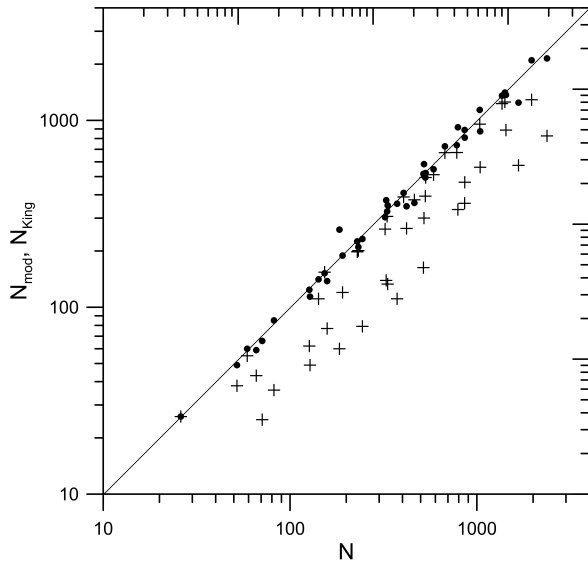


Figure 14. Comparison of the values N_{mod} (the cluster star number in the combined model) and N_{King} (the cluster star number in the King model) against the values of N (the cluster star number from the visual estimate of parameters), shown for different limiting magnitudes for each sample cluster. The filled circles are N_{mod} values, and crosses are N_{King} values.

bers of cluster stars for magnitude intervals of 1 mag width were calculated (and their uncertainties). Then these numbers were multiplied by the mean stellar masses obtained from the data of Table 9, for every magnitude interval. The mass of the cluster stars from the upper magnitude interval was estimated with the assumption of the Kroupa mass spectrum (Kroupa 2001) in this interval (see below in this Section). Finally, the cluster mass estimates were obtained as the sum of the masses for all magnitude intervals. The obtained cluster masses are the lower estimates, because the unknown low-mass end of stellar mass distribution, unresolved binaries and prob-

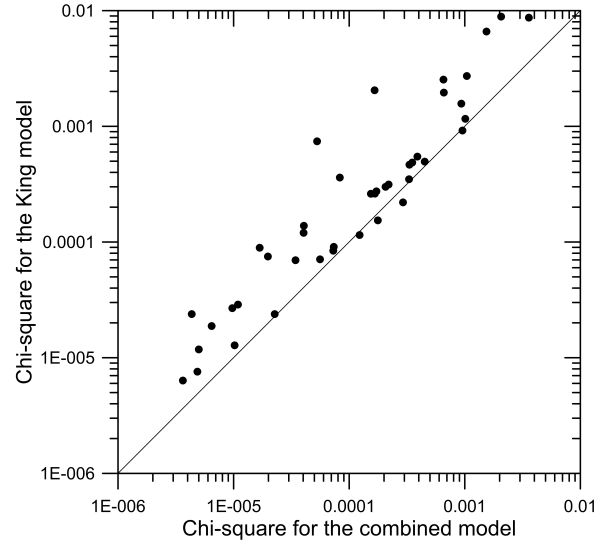


Figure 15. Comparison of the chi-square parameters for the King model approximation against the chi-square parameters for the combined model approximation.

able remnants of massive stars, are not taken into account. These lower estimates of the sample cluster masses are listed in the second column of Table 12. In the case of NGC 2287, the estimate of its mass was carried out only up to $J_{\text{lim}} = 15$ mag, because in the case of NGC 2287 the cluster star number with $J_{\text{lim}} = 16$ mag is smaller, than the cluster star number with $J_{\text{lim}} = 15$ mag (see Table 11). This fact can be explained by the large-scale fluctuations of the stellar background density. It could result in the wrong (higher) estimate of the surface density of the stellar background, and, as a consequence, in the wrong (lower) estimate of the cluster star number in the case of $J_{\text{lim}} = 16$ mag.

The total cluster mass, that was not covered by the method adopted here, can be estimated. NGC 1502 is taken as the only example. The following assumptions and approaches were used.

1. The mass interval for stars included into star counts is [0.4; 17.3] solar masses. These values are taken from Table 9. The mass interval for low-mass (unseen) stars is [0.08; 0.4] solar masses. The initial mass interval of the massive stars, finished their evolution already, is [17.3; 60.] solar masses.

2. Kroupa initial mass spectrum (Kroupa 2001) is adopted for these mass intervals:

$$\phi(m) \sim \begin{cases} m^{-1.3 \pm 0.5} & \text{with } m \in [0.08; 0.5], \\ m^{-2.3 \pm 0.3} & \text{with } m > 0.5. \end{cases}$$

3. The number of the stars in the mass interval of $[m_1; m_2]$ is

$$N = \int_{m_1}^{m_2} \phi(m) dm,$$

the mass of the stars in the same mass interval is

$$M = \int_{m_1}^{m_2} m \phi(m) dm.$$

4. The normalization constant of the Kroupa initial mass spectrum is determined, because the number of the cluster stars in the mass range of [0.4, 17.3] (taken from Table 9) is 860 (Table 11).

5. The open cluster NGC 1502 is young (see Table 1), and

Table 12. Lower estimates of the sample cluster masses and tidal radii

Cluster name	Lower estimate of cluster mass M, M_{\odot}	Lower estimate of tidal radius R_t, pc	$R_{c \text{ max}},$ pc	$R_{2 \text{ max}},$ pc
NGC 1502	1300±140	14.1±1.2	13.3±2.2	12.9±0.2
NGC 1960 (M 36)	860±100	12.3±1.0	8.8±1.1	8.8±0.2
NGC 2287 (M 41)	880±150	12.6±1.2	11.6±1.8	9.8±0.1
NGC 2516	1820±200	15.4±1.3	11.2±0.5	10.8±0.04
NGC 2682 (M 67)	1400±110	15.1±1.2	15.1±1.3	13.8±0.2
NGC 6819	1890±140	16.7±1.3	22.7±2.7	23.3±0.7
NGC 6939	2610±420	18.3±1.7	37.6±3.6	49.0±0.7

the fraction of low-mass stars lost by the cluster due to relaxation is negligible, see, for example, Ernst et al. (2015). For the intermediate-aged and old clusters the star escapes should be considered, but the procedure of the total mass evaluation was applied to NGC 1502 only, as the example.

6. The stars with the initial masses within the range of [17.3; 60.] solar masses become the neutron stars or black holes in the dependence of the concrete initial mass value, see Heger et al. (2003). The masses of the stellar remnants can be evaluated with the data from Heger et al. (2003).

7. The uncertainties of the estimates are evaluated by variation of the exponents of the mass spectrum within the ranges [-1.8;-0.8] and [-2.6;-2.0], and by taking into account the uncertainties of the stellar masses from Table 9, and the uncertainty of the cluster star number from Table 11.

8. The presence of unresolved binary stars can be taken into account following Khalaj & Baumgardt (2013) and supposing, for example, the same binary fraction as in the Praesepe cluster (0.35). In that case the coefficient 1.35 should be applied to the mass estimate.

Applying these steps to NGC 1502 gives the estimate of NGC 1502 total mass between approximately 1760 and 3900 solar masses. The uncertainty of this estimate is very large. Moreover, the fraction of the unresolved binary stars can vary in the range from 0.3 to 0.5 (Sollima et al. 2010). Due to large uncertainty, this procedure was not applied to the sample clusters; it was preferred to use the lower mass estimates listed in Table 12 for all sample clusters (including NGC 1502).

With this lower estimates of the sample cluster masses, the lower estimates of the cluster tidal radii in the Galactic gravitational field were calculated. The model of Galactic gravitational potential Φ was used from Kutuzov & Osipkov (1980). The following formula was used for the tidal radii estimate (King 1962):

$$R_t = \left(\frac{GM}{4A(A-B)} \right)^{1/3} = \left(-\frac{GM}{\alpha_1} \right)^{1/3}. \quad (16)$$

Here G is the gravitational constant, $G = 0.004535$ in the unit system 1 pc for distance; 1 M_{\odot} (one solar mass) for mass; and 1 Myr for time, as adopted in the present work. M is the cluster mass; A and B are Oort's constants for the cluster Galactocentric distance R_{cl} ; α_1 is the parameter describing the Galactic potential at the current Galactocentric distance of the cluster (introduced by Chandrasekhar (1942)):

$$\alpha_1 = R \left(\frac{1}{R} \frac{\partial \Phi}{\partial R} - \frac{\partial^2 \Phi}{\partial R^2} \right) \Big|_{R=R_{cl}}, \quad (17)$$

where R is the distance from the Galactic centre and R_{cl} is the cluster distance from the Galactic centre.

$$R_{cl} = \sqrt{R_0^2 + d^2 \cos^2 b - 2R_0 d \cos l \cos b}, \quad (18)$$

where R_0 is the Solar distance from the Galactic centre ($R_0 = 8200$ parsecs value was taken here, see, for example, Nikiforov (2004) and Hou & Han (2014)), l and b are the galactic coordinates of the cluster, and d is the cluster distance from the Sun. With the Kutuzov & Osipkov (1980) model,

$$\alpha_1 = -2\Phi_0 \left(\frac{R_{cl}}{R_a} \right)^2 \frac{1+3e}{e^3(1+e)^3}, \text{ and} \quad (19)$$

$$e = \sqrt{1 + \left(\frac{R_{cl}}{R_a} \right)^2},$$

where $R_a = 2000$ pc, and $\Phi_0 = 1.841 \cdot 10^5 \text{ pc}^2/\text{Myr}^2$.

The Galactic potential model of Kutuzov & Osipkov (1980) was chosen on the following considerations. In order to derive the open cluster tidal radii, the model of Galactic potential is needed, that well describes the Galactic potential in the Solar vicinity in the Galaxy, because all the sample clusters are close to the Sun ($d < 2.36$ kpc). The compatibility of the Oort constants A and B derived from the model and modern data on the A and B can be a criterion. Bobylev & Bajkova (2014) determined $A = 16.49 \pm 0.60$ km/s/kpc and $B = -12.37 \pm 1.12$ km/s/kpc with the study of high precision data on the 73 maser sources. These values give $4A(A-B) \simeq 1900 \text{ km}^2/\text{s}^2/\text{kpc}^2$. The constants A and B derived from the Kutuzov & Osipkov (1980) model with $R_0 = 8200$ parsecs are $A = 17.08$ km/s/kpc and $B = -10.58$ km/s/kpc. These values give $4A(A-B) \simeq 1890 \text{ km}^2/\text{s}^2/\text{kpc}^2$, that is very close to the value from Bobylev & Bajkova (2014).

The Solar Galactocentric distance of $R_0 = 8200$ parsecs is the reasonable value, compatible with the modern data, see the reviews in Nikiforov (2004) and Hou & Han (2014).

The modern models of the Galactic potential are aimed at the determination of the Galactic extended dark halo parameters, see, for example, Bonaca et al. (2014). The perturbations are added to the potential, that are connected with the presence of the bar and the spiral arms, see the review in Pettitt et al (2014). But the Galactic potential model of Kutuzov & Osipkov (1980) is relatively simple, and gives the adequate values of the Oort constants in the Solar vicinity, and it is sufficient for the present work.

The lower estimates of the sample cluster tidal radii are listed in the third column of Table 12. The uncertainty of this estimate

was obtained taking into account the uncertainty of the cluster mass estimate, the uncertainty of the cluster distance from the Sun, and a 10% uncertainty of the R_0 value.

The fourth column of Table 12 contains a maximum visual estimate of the cluster radius for all magnitude intervals. The fifth column of Table 12 contains the maximum corona radius for all magnitude intervals, obtained by the cluster surface density profile approximation with the combined model. It is seen that NGC 6819 and NGC 6939 extend well beyond their tidal surfaces. This fact is unlikely to be changed due to the unknown low-mass tail of stellar content in these clusters and to unresolved binaries, because Eq.(16) contains the cluster mass to the $1/3$ power. Then an increase of the cluster mass by two times will lead to a tidal radius increase by only a 1.26 factor. The large extension of these clusters can be explained by their non-stationarity: the rapid expansion of the cluster and the stabilizing ejections of the cluster stars into galactic field (see Danilov (1982, 2005, 2011)).

The young and intermediate-age clusters can be subjected to the influence of additional gravitational action from the nearest gas-star complex with concomitant movement relative to the cluster (that is the gas-star complex where the cluster has been formed). This action leads to a decrease in the cluster tidal radius of a factor of 1.5-2.5 (Danilov 1990). Taking into account this possibility, it can be so explained why young and intermediate-age clusters from our sample show the same evidence of non-stationary processes (see Fig.11) as old clusters NGC 6819 and NGC 6939, which extend over their tidal surfaces.

8 CONCLUSIONS

The purpose of the present study was to show the efficiency of kernel estimation of surface and spatial density profiles of open star clusters and their N-body models, especially in the outer cluster region, and to demonstrate the necessity of taking into account the corona component of the open cluster when choosing the model for the surface density profile approximation.

The following general results were obtained in the present research.

1. The formulae for kernel estimates of spatial density profiles of star clusters were obtained, for the cases when stellar spatial coordinates (x,y,z) are known. Spatial density profiles for N-body models of open cluster coroneae were derived as examples. The result of Danilov et al. (2014) was confirmed concerning the formation of quasi-equilibrium density distribution in the open cluster coroneae up to distances of three tidal radii from the cluster centre.

2. Surface density profiles were derived for seven open clusters for different limiting magnitudes using the data of 2MASS. The optimal kernel halfwidth value was selected following Merritt & Tremblay (1994), it was the value, that gave the smoothest curve that closely followed the mean trend defined by curves computed with much smaller kernel halfwidth. The surface density of the stellar background and cluster radii were estimated by the surface density profile. It was shown that the cluster radius estimate is hardly dependent on the kernel halfwidth value, when it is less or equal to the optimal one. The comparison with other investigations shows that data on open cluster sizes are often underestimated. The result of Artyukhina & Kholopov (1965) was confirmed about the presence of an extended corona in the open cluster NGC 6939.

3. The surface density profiles of the sample clusters show evidence of mass segregation and irregularities in the outer parts

of clusters which can be interpreted as evidence of non-stationary processes in the clusters.

4. The surface density profiles of the sample clusters were approximated by the King function and by the combined model; that is, a combination of the King function for the cluster core and the uniform sphere for representation of the cluster corona. It is shown that the combined model describes surface density profiles of the sample clusters much better than the King model alone. This is especially well seen when the cluster star numbers, obtained by integration of the surface density profiles from the kernel estimates and its models, are compared.

5. The lower estimates of the sample cluster masses and tidal radii in the Galactic gravitational field were obtained. It is shown that open clusters NGC 6819 and NGC 6939 extend beyond their tidal radii. This can be explained by their non-stationarity: by rapid expansion of these clusters and by the stabilizing ejections of the cluster stars into the galactic field.

ACKNOWLEDGMENTS

The author is very grateful to Prof. D.Merritt for introducing him to the kernel estimator method, and to Prof. V.M.Danilov for helpful discussions. The author also acknowledges the assistance of Dr. T.P.Rasskazova and Mr. Ian Miller (Dept. Foreign Languages, INS, UrFU) in the preparation of this article. This work was partially supported by the Ministry of Education and Science of the Russian Federation (state contract No. 3.1781.2014/K, registration number 01201465056). The travel to the conference was supported by Act 211 Government of the Russian Federation, agreement No. 02.A03.21.0006. This publication makes use of data products from the Two Micron All Sky Survey, which is a joint project of the University of Massachusetts and the Infrared Processing and Analysis Center, California Institute of Technology, funded by the National Aeronautics and Space Administration and the National Science Foundation.

REFERENCES

- Alves V.M., Pavani D.B., Kerber L.O., Bica E., 2012, *New Astr.*, 29, 488
 Artyukhina N.M., 1970, *SvA*, 14, 130
 Artyukhina N.M., Kholopov P.N., 1962, *SvA*, 5, 796
 Artyukhina N.M., Kholopov P.N., 1965, *Soobsh. Gos. Astron. Inst. Stern.*, 142-143, 3 (in Russian)
 Balaguer-Núñez L., Jordi C., Muiños J.L., Galadí-Enríquez D., Masana E., 2013, *High. Span. Astrophys. VII. Proc. X Sci. Meet. Span. Astron. Soc.*, 644
 Belikov A.N., Hirte S., Meusinger H., Piskunov A.E., Schilbach E., 1998, *A&A*, 332, 575
 Bergond G., Leon S., Guibert J., 2001, *A&Ap*, 377, 462
 Bessell M.S., Brett J.M., 1988, *PASP*, 100,1134
 Bobylev V.V., Bajkova A.T., 2014, *Astron.Lett.*, 40, 389
 Bonaca A., Geha M., Küpper A.H.W., Diemand J., Johnston K.V., Hogg D.W., 2014, *ApJ*, 795,94
 Bressan A., Marigo P., Girardi L., Salasnich B., Dal Cero C., Rubele S., Nanni A., *MNRAS*, 2012, 427, 127
 Camargo D., Bonatto C., Bica E., 2012, *MNRAS*, 423, 1940
 Carballo-Bello J.A., Gieles M., Sollima A., Koposov S., Martínez-Delgado D., Penarrubia J., 2012, *MNRAS*, 419, 14
 Carraro G., Zinn R., Moni Bidin C., 2007, *A&Ap*, 466, 181

- Carraro G., Seleznev A.F., 2012, *MNRAS*, 419, 3608
- Chandrasekhar S., 1942, *Principles of Stellar Dynamics*. Univ. Chicago Press, Chicago, Ill
- Cutri R. M., et al., 2003, *Explanatory Supplement to the 2MASS All Sky Data Release*. NASA, Washington, <http://www.ipac.caltech.edu/2mass/releases/all-sky/doc/explsup.html>
- Danilov V.M., 1982, *SvA*, 26, 297
- Danilov V.M., 1990, *SvA*, 34, 124
- Danilov V.M., 2005, *Astron.Rep.*, 49, 604
- Danilov V.M., 2011, *Astron.Rep.*, 55, 473
- Danilov V.M., Dorogavtseva L.V., 2008, *Astron.Rep.*, 52, 467
- Danilov V.M., Matkin N.V., Pylskaya O.P., 1985, *SvA*, 29, 621
- Danilov V.M., Putkov S.I., 2012, *Astron.Rep.*, 56, 609
- Danilov V.M., Putkov S.I., Seleznev A.F., 2014, *Astron.Rep.*, 58, 906
- Danilov V.M., Seleznev A.F., 1994, *Astron. Astrophys. Trans.*, 6, 85
- Davenport J.R.A., Sandquist E.L., 2010, *ApJ*, 711, 559
- Djorgovski S., 1988, in Grindlay, J.E., Philip, A.G.Davis, eds, *Proc. IAU Symp. 126, The Harlow-Shapley Symposium on Globular Clusters Systems in Galaxies*. Kluwer Academic Publishers, Dordrecht, p.333
- Ernst A., Berczik P., Just A., Noel T., 2015, [arXiv:1506.02862](https://arxiv.org/abs/1506.02862)
- Gennaro M., Brandner W., Stolte A., Henning Th., 2011, *MNRAS*, 412, 2469
- Goldman B. et al., 2013, *A&A*, 559, 43
- Heger A., Fryer C.L., Woosley S.E., Langer N., Hartman D.H., 2003, *ApJ*, 591, 288
- Hou L.G., Han J.L., 2014, *A&A*, 569, A125
- Khalaj P., Baumgardt H., 2013, *MNRAS*, 434, 3236
- Kharchenko N.V., Piskunov A.E., Röser S., Schilbach E., Scholz R.-D., 2005, *A&A*, 438, 1163
- Kholopov P.N., 1963, *SvA*, 7, 89
- Kholopov P.N., 1969, *SvA*, 12, 625
- King I.R., 1962, *AJ*, 67, 471
- Kirsanova M.S., Sobolev A.M., Thomasson M., Wiebe D.S., Johansson L.E.B., Seleznev A.F., 2008, *MNRAS*, 388, 729
- Kroupa P., 2001, *MNRAS*, 322, 231
- Kutuzov S.A., Osipkov L.P., 1980, *SvA*, 24, 17
- Küpper A.H.W., Macleod A., Heggie D.C., 2008, *MNRAS*, 387, 1248
- Küpper A.H.W., Kroupa P., Baumgardt H., Heggie D.C., 2010, *MNRAS*, 401, 105
- Küpper A.H.W., Kroupa P., Baumgardt H., Heggie D.C., 2010, *MNRAS*, 407, 2241
- Laney C.D., Stobie R.S., 1993, *MNRAS*, 263, 921
- van Leeuwen F., 1980, in Hesser J., ed., *Proc. IAU Symp. 85, Star Clusters*. Reidel, Dordrecht, p.157
- van Leeuwen F., 2009, *A&A*, 497, 209
- Loktin A.V., Gerasimenko T.P., Malysheva L.K., 2001, *Astron. Astrophys. Trans.*, 20, 607
- Marquardt D., 1963, *J.Soc.Indust.Appl.Math.*, 11, 431
- Merritt D., Tremblay B., 1994, *AJ*, 108, 514
- Miocchi P. et al., 2013, *ApJ*, 774, 151
- Nikiforov I.I., 2004, in Byrd G., Kholoshevnikov K., Mylläry A., Nikiforov I., and Orlov V., eds, *ASP Conf. Ser. Vol. 316, Order and Chaos in Stellar and Planetary Systems*. Astron. Soc. Pac., San Francisco, p. 199
- Nilakshi, Sagar R., Pandey A.K., Mohan V., 2003, *A&A*, 383, 153
- Pancino E., Seleznev A., Ferraro F.R., Bellazzini M., Piotto G., 2003, *MNRAS*, 345, 683
- Pang X., Grebel E.K., Allison R.J., Goodwin S.P., Altmann M., Harbeck D., Moffat A.F.J., Drissen L., 2013, *ApJ*, 764, 73
- Pettitt A.R., Dobbs C.L., Acreman D.M., Price D.J., 2014, *MNRAS*, 444, 919
- Press W.H., Teukolsky S.A., Vetterling W.T., Flannery B.P., 1997, *Numerical Recipes in Fortran 77. The Art of Scientific Computing*. Second Edition. Volume 1 of Fortran Numerical Recipes. Press Syndicate of the University of Cambridge, New York, NY.
- Prisinzano L., Carraro G., Piotto G., Seleznev A.F., Stetson P.B., Saviane I., 2001, *A&A*, 369, 851
- Sanchez N., Alfaro E.J., 2009, *ApJ*, 696, 2086
- Santos-Silva T., Gregorio-Hetem J., 2012, *A&A*, 547, A107
- Skrutskie M.F. et al., 2006, *AJ*, 131, 1163
- Seleznev A.F., 1998, *Astron.Rep.*, 42, 153
- Seleznev A.F., Carraro G., Piotto G., Rosenberg A., 2000, *Astron.Rep.*, 44, 12
- Seleznev A.F., Carraro G., Costa E., Loktin A.V., 2010, *New Astron.*, 15, 61
- Silverman B.W., 1986, *Density Estimation for Statistics and Data Analysis*. Chapman & Hall, London
- Sollima A., Carballo-Bello J.A., Beccari G., Ferraro F.R., Pecci F.Fusi, Lanzoni B., 2010, *MNRAS*, 401, 577
- Sosin C., King I.R., 1995, *AJ*, 109, 639
- Sosin C., King I.R., 1997, *AJ*, 113, 1328
- Sung H., Sana H., Bessell M.S., 2013, *AJ*, 145, 37
- Vesperini E., McMillan S., Portegies Zwart S., 2009, *Ap&SS*, 324, 277
- Walton N.A., et al., 2012, in Aoki W., Ishigaki M., Suda T., Tsujimoto T., and Arimoto N., eds, *ASP Conf. Ser. Vol.458, Galactic Archaeology: Near-Field Cosmology and the Formation of the Milky Way*. Astron. Soc. Pac., San Francisco, p.419
- Yang S.-C., Sarajedini A., Deliyannis C.P., Sarrazine A.R., Kim S.C., Kyeong J., 2013, *ApJ*, 762, 3